

Impact of Basalt Powder on the Physical, Fresh, Hardened and Microstructural Characteristics of Granulated Blast Furnace Slag-Based Alkali-Activated Mortars

Merve Şahin Yön^{1*} , Selim Cemalgil¹ 

¹Munzur University, Faculty of Engineering, Department of Civil Engineering, Tunceli, Türkiye, mervesahinyon@munzur.edu.tr, scemalgil@munzur.edu.tr, ror.org/05v0p1f11

*Corresponding Author

ARTICLE INFO

ABSTRACT

Keywords:

Basalt powder
Alkali-activated mortar
Physical properties
Mechanical properties



Article History:

Received: 03.08.2025
Revised: 22.10.2025
Accepted: 26.11.2025
Online Available: 28.01.2026

In this study, the workability, mechanical and physical aspects of alkali-activated mortar (AAM) containing basalt powder (BP) and granulated blast furnace slag (GBFS) were investigated. For the experimental study, alkali-activated mortars (AAM) containing BP at 8%, 16%, 24%, 32% and 40% substitution rates for GBFS were developed. Mortars were synthesized with a sodium silicate/sodium hydroxide ratio of 3.0 for the binder materials and a 0.45 alkali activator-to-binder ratio. The flow diameters of the fresh mortars prepared using 40x40x160 mm molds were determined according to the European Federation of Experts in Construction Chemicals and Concrete Systems (EFNARC) standard. The fresh AAMs were wrapped in stretch film to prevent evaporation and then kept in an oven at 60°C for 48 hours. The cured samples were evaluated for their mechanical strengths at 3 and 28 days, freeze-thaw effects after 33 and 100 cycles, and microstructures after 100 cycles. According to the results, using 40% BP instead of GBFS caused a decrease of approximately 15.08% in 28-day compressive strength compared to the reference sample (100% GBFS). G100 showed a minimum porosity of 15.81% and a water absorption rate of approximately 7.3%. The G60B40 mixture had the highest sorptivity capacity with 5.29×10^{-3} cm/s^{0.5}, while the G100 mixture showed the lowest capacity with 3.88×10^{-3} cm/s^{0.5}. After 100 freeze-thaw cycles, the G60B40 sample had the largest strength loss of 61.61%, while the G100 sample showed the lowest strength loss of 9.89%.

1. Introduction

The structure industry is among the most rapidly expanding sectors worldwide. Portland cement, the principal binding agent utilized in this industry, leads to substantial loss of natural resources and considerable carbon dioxide emissions. The operations of cement manufacturing and utilization, which generate 1.35 billion tons of CO₂ annually, constitute about 8% of global emissions [1, 2]. Given these principles, the notion that cement consumption should be diminished to lower CO₂ emissions underscores the need of sustainable technologies for producing new materials with decreased CO₂ emissions [3, 4]. Furthermore, the environmentally friendly disposal of industrial

byproducts such as fly ash [5], granulated blast furnace slag [6], silica fume, metakaolin [7, 8], and marble dust [9] is a separate issue. Consequently, the creation of sustainable alternatives to conventional cement-based mortars is critically significant [10].

Geopolymers [11] have attracted increasing attention from researchers as an alternative to Portland cement, which causes greenhouse gas emissions during its production. It is regarded as a minimum two-component, inorganic system, constituted by a combination of a solid precursor material in SiO₂ and Al₂O₃ and one or more alkaline activator solutions [12]. These mortars are produced by activating silicon-rich solid precursor materials (metakaolin [13], slag [14,

15], silica fume, fly ash etc.) with alkali activators such as alkali hydroxide, carbonate or silicate [16]. Well-formulated alkali-activated mortars have a more compact microstructure and enhanced engineering qualities [17] relative to mortars or concrete made with conventional cement. Nonetheless, limiting clinker production mitigates CO₂ emissions and reduces energy usage [18].

Recently, sustainable mortar or concrete production has become the focus of researchers. Wankhede and Ralegaonkar conducted a study to formulate alkali activated foundry sand mortar (OAFSM) with foundry waste sand (FWS) for sustainable solid waste management. Blast furnace slag fine powder (BFSFP) and fly ash (FA) were utilized in varying amounts as solid precursors, while sodium metasilicate (SM) served as the solid activator. FWS was utilized in quantities of 0%, 25%, 50%, 75%, and 100% in lieu of traditional fine aggregate. The study shown that the blended mixtures significantly enhanced the mechanical properties of the mortar. The rise in BFSFP content resulted in enhanced compressive and flexural strengths [19].

Mobili et al. synthesized alkali-activated mortar utilizing copper mine tailings (CMT) and metakaolin (MK). Findings indicate that utilizing CMT with 25% MK by mass is appropriate, achieving a compressive strength exceeding 30 MPa. It was determined that mortars composed entirely of MK had significant resistance against sulfate attack [20]. Ma et al. sought to achieve entirely recycled alkali-activated materials by substituting ground granulated blast furnace slag (GGBS)-fly ash and natural sand with waste concrete fines as binders. Researchers noted that Waste Concrete Fine (WCF) has significant alkali activation properties and a filling effect in mortar. Substituting binders with WCF adversely impacts geopolymerization and compromises the microstructure of the paste, whereas substituting natural sand with WCF enhances the microstructure of AAM paste by decreasing the actual water-binder ratio [21].

Guo et al. synthesized alkali-activated binders by amalgamating sulphurous iron ore waste (SIOT) with metakaolin (MK) and GGBS. The findings

indicated that alkali activators with an SH molarity exceeding 10M and a SiO₂/Na₂O ratio ranging from 0.86 to 1.3 successfully produced SEM crystalline C-A-S-H gel to encapsulate SIOT particles, hence offering robust pore-filling and bonding characteristics. These mixes exhibited enhanced compressive and flexural strengths, excellent freeze-thaw resistance, and diminished drying shrinkage [22]. Yurt and Bayraktar investigated the effect of alkali activator concentration in geopolymer mortars containing waste brick dust. Researchers found that the highest compressive strength was achieved in mixtures with a 0.45 NaOH/ (NaOH + Na₂SiO₃) ratio and an activation temperature of 60°C [23].

Another experimental research examined the impact of alkali activators, formulated with 12 M [24] NaOH and silicate with a silica modulus of 3.22, on the performance of mortars produced by substituting GBFS and BP. Mrozek et al. concluded that basalt powder alone could not synthesize alkali-active products based on their preliminary trial mixtures. Therefore, they further tested the mixture by substituting 10% and 20% of the total binder weight with metakaolin [25]. Researchers have established that the influence of BP mixing ratios on material strength is intricate. Consequently, determining the correct quantity of BP is essential, as excessive quantities may result in structural deficiencies [26, 27].

The substitution rates of BP were established based on prior research concerning additions like slag, fly ash, and metakaolin utilized in alkali-activated systems. Substitution rates ranging from 10% to 40% were chosen based on existing literature to evaluate the impact of the lower and higher thresholds of the BP rate on both fresh and hardened characteristics. Experimental studies were conducted using BP at 0%, 8%, 16%, 24%, 32%, and 40%, respectively, instead of GBFS, according to literature. Laboratory investigations included flowability testing, 3- and 28-day compressive-flexural strength assessments, freeze-thaw durability assessment, capillary water absorption measurement, total water absorption analysis, porosity determination, ultrasonic pulse velocity tests, and microstructure assessment.

The difference of this study from other studies is that the mechanical strength and freeze-thaw effect of the environmentally friendly alkali-activated mortar produced using BP and GBFS were evaluated through comprehensive experiments.

2. Experimental Research

The flow chart in the Figure 1 shows the steps of this study.

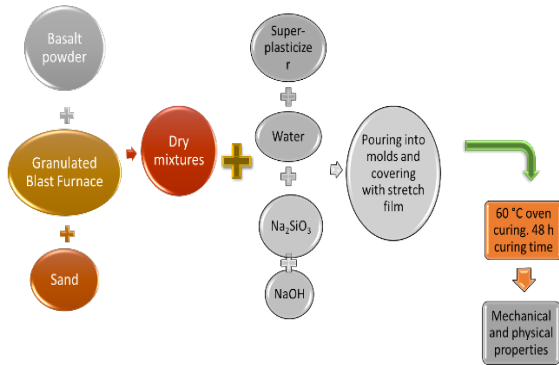


Figure 1. Flow chart

2.1. Material and method

Following the provision of BP and GBFS identified as binder precursor materials were ground to 75 μm particle size for 20 hours using a Los Angeles aggregate abrasion apparatus. X-ray diffraction (XRD) graph of BP and GBFS is given in Figure 2. The XRD patterns of the products were obtained using a Rigaku Miniflex600 diffractometer. Specimens were irradiated with Cu-K α radiation at a voltage of 40 kV and a current of 15 mA. XRD investigations were performed at a wavelength of 1.5406 (λ) within the range of 10 to 90 degrees, with a step increment of 0.02 degrees and a scanning speed of 2 degrees per minute. The peaks identified in the phase analysis of BP include Andesine, Anorthoclase, Albite, and SiO₂, whereas the peaks associated with GBFS comprise Akermanite, Merwinite, and Gehlenite. The inclusion of GBFS, which possesses a high reactive amorphous content and is abundant in SiO₂ and calcium sources essential for AAM formation, enhances the characteristics of the binder when combined with BP that has a low calcium concentration [28, 29].

Figures 3a and 3c illustrate the FIB-SEM images of BP and GBFS, respectively, under 5000 magnifications. The FIB-SEM picture of BP reveals uneven, fractured, and angular particles with grain sizes of around 3.149 μm , 4.805 μm and 4.861 μm , as depicted in Figure 3a. In Figure 3c, irregular angled particles are seen in the FIB-SEM images of GBFS with grain sizes of 9.759 μm , 16.45 μm and 9.559 μm . Figures 3b and 3d demonstrate the EDS analyses of BP and GBFS, respectively. Figure 3b illustrates the weight distributions of the predominant elements in the EDS images of BP (O 46.7%, Si 19.7%, and Al 8.8%).

Additionally, the weight distributions of the predominant elements in the EDS pictures of GBFS (O 44.2%, Si 13.6%, and Ca 22.6%) are illustrated in Figure 3d. The chemical contents of BP and GBFS samples are given in Table 1. For chemical analysis, the main oxides similar to cement are given. Elements such as hydrogen, carbon, sulphur and Cl are not included in the report. All dry materials used in this study are shown in Figure 4. Fine material for the tests was sourced from river sand in the Elazığ (Palu) region. The specific gravity of the sand within the 0-4 mm range was 2.63, and the water absorption rate was 1.96. Figure 5 illustrates the gradation graph of the aggregate.

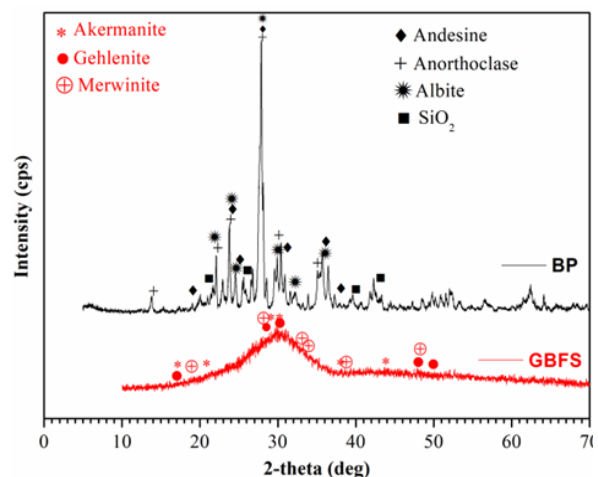


Figure 2. XRD graph of BP and GBFS

A 12M NaOH solution was made using sodium hydroxide pellets. Sodium silicate solution with a silica modulus of 3.22 was used. The sodium silicate liquid utilized in all AAM combinations comprised the following mass percentages: 62.0% H₂O, 28.425% SiO₂ and 8.835% Na₂O resulting in a silica modulus (SiO₂/Na₂O) of 3.22.

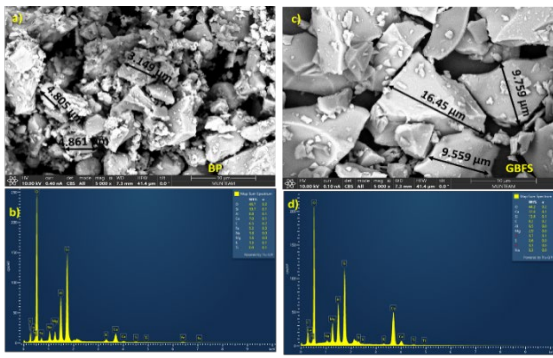


Figure 3. FIB-SEM/EDS images of a-b) BP and c-d) GBFS

Table 1. Chemical analysis results of BP and GBFS

Component name	% Component BP	% Component GBFS
SiO ₂	48.10	38.95
Al ₂ O ₃	15.86	15.78
Fe ₂ O ₃	9.00	0.91
CaO	7.23	36.37
MgO	7.35	6.35
Na ₂ O	4.09	0.43
K ₂ O	1.78	0.56
SO ₃	0.06	-
Specific Gravity	2.63	2.89



Figure 4. Dry materials

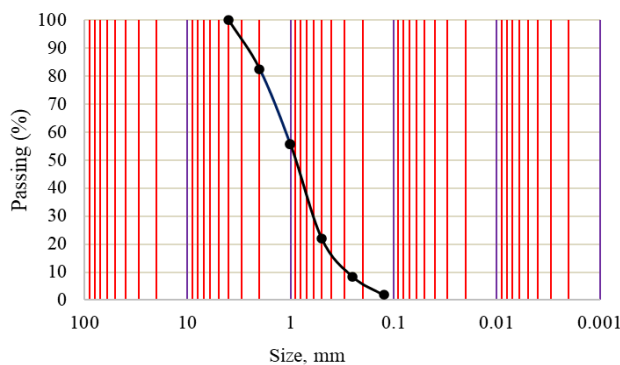


Figure 5. Gradation curve of river sand

The newly mixed mortar poured into the molds was covered with stretch film to inhibit air infiltration. Hardjito et al. asserted that while

compressive strength at elevated curing temperatures improves with age, there is no considerable enhancement in strength at curing temperatures over 60°C or durations surpassing 48 hours [30]. Furthermore, a study conducted by Temujin et al. indicated that heat curing at 40°C and 80°C, along with a 48-hour curing duration, are critical criteria for geopolymerization [31]. Therefore, a temperature of 60°C and a duration of 48 hours were favored in this investigation. The samples were stored in a stretch-covered manner in room settings until mechanical and physical testing days of 3 and 28 days.

The mixing ratios of the prepared AAMs, utilizing an activator/binder ratio of 0.45, are presented in Table 2. The water/binder ratio is fixed and is 0.20. The quantities of water and SP in all mixes are specified at 116 kg/m³ and 8 kg/m³, respectively. In this study, a fixed water/binder ratio was used. The manufacture of the mixture commenced with manual blending of the dry constituents (fine aggregate and binders) for one minute until uniformity was achieved. Subsequently, pre-weighed sodium hydroxide, sodium silicate, water, and superplasticizer were incorporated into the dry mixture and blended at low speed for 1 minute, followed by medium speed for 2 minutes. The application of fresh mortar was conducted utilizing flow-cone experiments to assess filling capacity.

Table 2. Mix amounts of AAMs for 1 m³

Series	BP (kg)	GBFS (kg)	Sand (kg)	Alkaline activator	
				NS	NH
G100	0	580	1277.53	195.75	65.25
G92B8	46.4	533.6	1273.36	195.75	65.25
G84B16	92.8	487.2	1269.18	195.75	65.25
G76B24	139.2	440.8	1265.01	195.75	65.25
G68B32	185.6	394.4	1260.83	195.75	65.25
G60B40	232	348	1256.66	195.75	65.25

2.1.1. Fresh properties

The flow-cone test was conducted in accordance with the EFNARC standard [32].

2.1.2. Mechanical tests

The fresh AAMs were cast in dimensions of 40×40×160 mm, adhering to ASTM C348 [33], from which both flexural and compressive strengths are obtained. The compressive

strengths were assessed by exposing the split samples to ASTM C349 [34]. The following equations (1) and (2) were employed to compute the strength values.

$$\sigma_f = \frac{3PL}{2bh^2} \quad (1)$$

$$\sigma_c = \frac{P}{A} \quad (2)$$

In Eq. (1), σ_f demonstrates stress at the midpoint of the beam (MPa), P indicates force at the centre of the load deflection curve (N), L shows distance between two support rollers (mm), b is the beam width and h are the beam height (mm).

In equation (2), σ_c compressive strength (MPa), A represents the sample's cross-sectional area (40 mm²), and P is the maximum refraction load (N).

2.1.3. Sorptivity, water absorption and density tests

Measurements of sorptivity, density, and water absorption were conducted after 28 days on samples measuring 50×50×50 mm (Figure 6). Considering the ASTM C1585 standard [35], sorptivity experiments were performed.

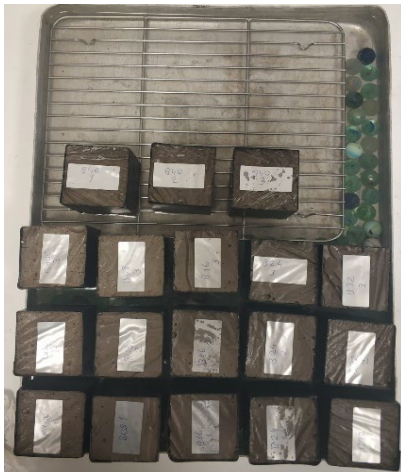


Figure 6. Sorptivity test specimens

2.1.4. Freeze-thaw test

Fifty freeze-thaw cycles were performed on eighteen samples using freeze-thaw testing apparatus (Figure 7), in compliance with ASTM C666 standards [36]. The operational principle of one cycle is as follows: the temperature of the mixes declined from +20 to -20 °C during a 6-hour duration, while the samples were immersed in water for 2 hours during the thawing process.



Figure 7. Freeze-thaw test device

2.1.5. FIB-SEM/EDS test

Surface morphologies of the materials were determined using FIB-SEM. Scanned areas were analysed by EDS using an Oxford Instruments AZtec EDS instrument.

3. Results and Discussion

3.1. Flow-cone test

Flow-cone experiments were performed to assess the workability and consistency characteristics of six fresh mortars using GBFS and BP. As seen in the Figure 8, the reference sample, G100 (100% GBFS, devoid of BP), demonstrated the greatest flow diameter of 260 mm, signifying superior workability compared to all other mixes. A rise in BP proportion and a drop in GBFS quantity resulted in a progressive reduction in flow diameter. The findings demonstrated that the mixtures with 32% and 40% BP exhibited satisfactory workability, albeit they fell beyond the spreading ranges outlined by EFNARC. The flow-cone diameters of the mixtures with 0, 8, 16, and 24% BP conformed to the slump flow reference values of 240-260 mm as proposed by EFNARC.

The diminished reactivity of BP relative to GBFS has resulted in decreased flowability, necessitating additional water or activator to get comparable fluidity [27]. In this study, "reactivity" denotes the diminished chemical activity of BP in comparison to GBFS. The reductions in fluidity cannot be exclusively ascribed to chemical activity; the physical characteristics of BP, including increased specific surface area and roughness, are also significant. An increased quantity of BP

enhances the total surface area, hence elevating water requirements. In this study, a fixed water/binder ratio was used.

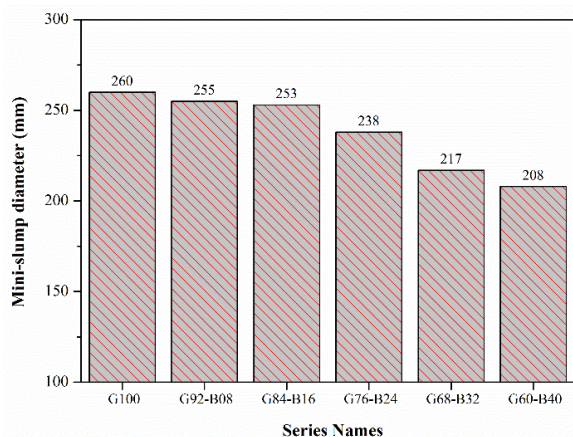


Figure 8. Flow-cone values

3.2. Mechanical experiments

Figure 9 illustrates 3- and 28-days average compressive strength values for mortar combinations including BP and GBFS. The compressive strength at 3 and 28 days diminishes with increasing BP concentration, except for the sample containing 8% BP, which exhibits an increase. This aligns with the research conducted by Rashad et al. [37], which indicates that prolonging the curing duration enhances the resultant compressive strength value. It is observed that the compressive strength values obtained at 28 days are higher with the increase in BP contribution, contrary to the value reported in [38].

The recorded maximum compression strength exceeded the reference sample (G100) in the 3 and 28-day ages G92B8 reached 53.06 and 54.77 MPa, respectively. The incorporation of 40 %BP relative to the reference sample resulted in a reduction of 15.08 % in the 28-day compressive strength. In reference to Figure 8, an increase in BP quantity elevates the overall water demand by diminishing fluidity. This enhances the porosity of the mixture. Figure 9 further substantiates this scenario. Therefore, this action adversely affected compressive strength.

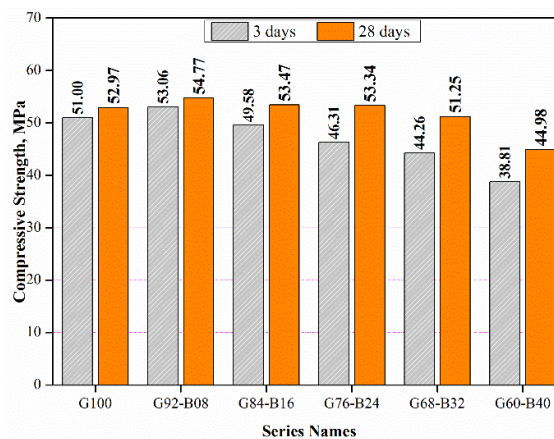


Figure 9. Compressive strength of specimens

3 and 28-day flexural strength of the samples is shown in Figure 10. While the 3-day flexural strength varies between 2.95 and 3.46 for all series, the flexural strength of the 28-day series varies between 3.35 and 4.66 MPa. The BP ratio exhibited a somewhat declining tendency at early ages, whereas it demonstrated a little increase in 28-day strengths. Accordingly, B40 exhibited a 14.7% decrease in 3-day flexural strength compared to the G100 control mixture. However, the highest flexural strength of 28 days was seen in the G60-B40 sample. The flexural strength in this sample was measured as 4.66 MPa. The G60B40 sample with the highest BP ratio showed a 33.9% increase compared to the G100 control mixture.

As a result, the lowest 3-day flexural strength was measured as 2.95 MPa in the G60-B40 sample, while the highest 28-day flexural strength was determined in this sample. This indicates that the BP contribution gives the sample resistance over time. Çelikten and Çavuşoğlu's study revealed that 24-hour composites achieved almost 85% of their final strength after a span of 7 days. They indicated that these examples could be utilized in applications necessitating early formwork removal, such as the prefabrication sector [39]. In contrast to prior research, the diminished early age strength of mixes incorporating BP in this study is attributed to their material composition, the low early age reactivity of BP, and the gradual advancement of the geopolymerization process.

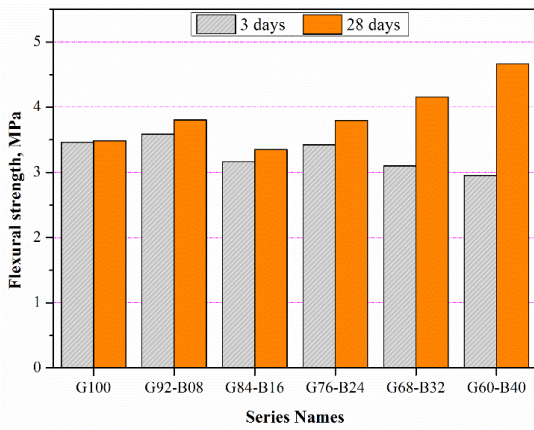


Figure 10. Flexural strength of specimens

3.3. Water absorption, density and sorptivity properties

Figure 11 illustrates the apparent porosity and water absorption values of AAMs with varying concentrations of GBFS and BP. G100 exhibited the lowest porosity at 15.81% and a water absorption rate of around 7.3%. As the BP ratio escalated from 8% to 40%, both porosity and water absorption values consistently rose. In the G60-B40 sample, porosity attained 20.15%, while water absorption approximated 9.9%. With the augmentation of BP content, porosity escalated. Enhanced porosity resulted in elevated water absorption values. This indicates that the mixture became more permeable and porous at 32% and 40% BP levels.

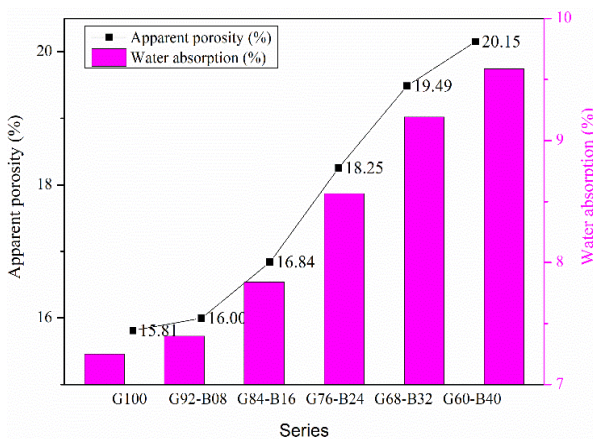


Figure 11. Porosity and water absorption

The apparent density and saturated surface-dry density (SSD) of the geopolymers samples are shown in Figure 12. This figure is important because it demonstrates that changes in BP ratios do not significantly alter the density of the samples. The stability of the density values implies that the replacement of BP does not

adversely impact the structural integrity of the matrix. This substantiates the appropriateness of BP as an additional material in alkali-activated systems. Moreover, the observed trend aligns with the findings of Servadei et al., hence corroborating the credibility of the results [40]. The apparent density values for the incorporation of 8%, 16%, 24%, 32%, and 40% BP by weight are 2.57 g/cm³, 2.58 g/cm³, 2.61 g/cm³, 2.63 g/cm³ and 2.63 g/cm³, respectively.

The increase in the basalt ratio contributed to the increase in the apparent density value. This is parallel to the study of Venyite et al [41]. Specimens G68B32 and G60B40 had the highest apparent density values at 2.63 g/cm³, whilst G92B8 displayed the lowest at 2.57 g/cm³. With the increase in BP concentration, slight reductions in SSD are noted. The reduction is 1.71% relative to G100 in the G60B40 sample exhibiting the greatest BP level. The minimum apparent and SSD densities in G60B40 indicate a weaker structure, corroborating a reduction in compressive strength.

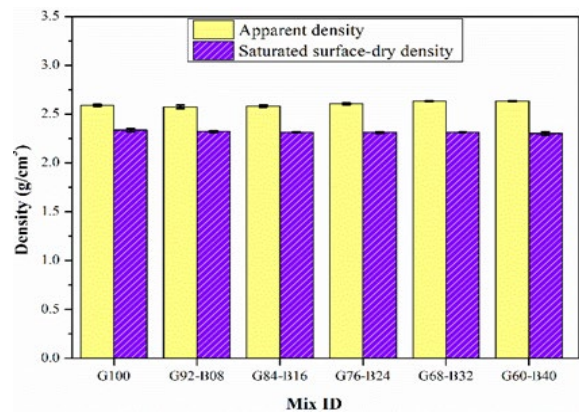


Figure 12. Density of samples

Sorptivity is a characteristic employed to readily ascertain porosity. This feature denotes water absorption and transfer via capillarity [42]. Figure 13 illustrates the sorptivity coefficients samples. This figure illustrates that an increase in the BP ratio and a decrease in GBFS resulted in an elevated sorptivity coefficient. The sample exhibiting the highest sorptivity coefficient is G60B40, with a value of $5.29 \times 10^{-3} \text{ cm/s}^{0.5}$. The minimum sorptivity coefficient value recorded for G100 was $3.88 \times 10^{-3} \text{ cm/s}^{0.5}$. The observation that GBFS exhibits the lowest water absorption coefficient aligns with findings from prior investigations [29, 43].

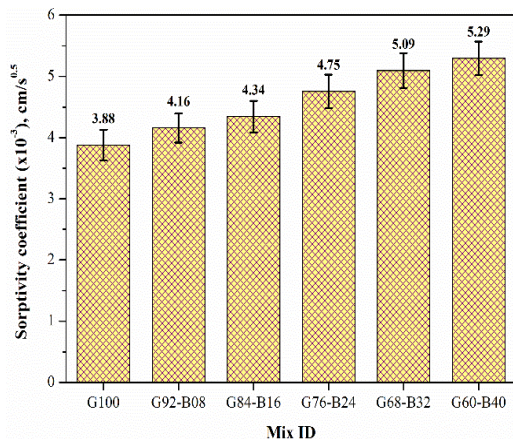


Figure 13. Sorptivity coefficient

3.4. Freeze-thaw resistance

Numerous researchers have put the mortars acquired to freeze-thaw testing across multiple cycles [44-46]. This investigation involved 18 samples with diverse BP contents (0-40%) exposed to 33 and 100 cycles, respectively. Figure 14 illustrates the mean weight variation following the cycle. Following 33 cycles, reductions of 1.87%, 2.09%, 2.1%, 2.2%, 1.93%, and 1.89% were seen in the G100, G92B8, G84B16, G76B24, G68B32, and G60B40 series, respectively. There was no change in weight from 33 to 100 cycles.

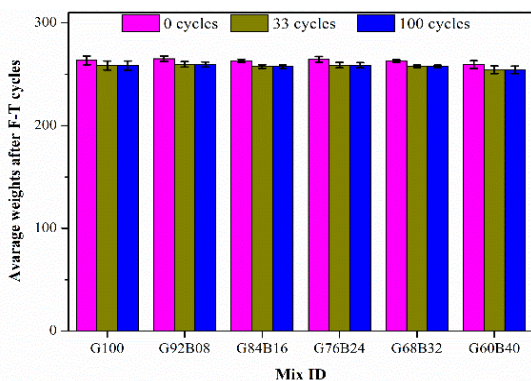


Figure 14. Average weights after F-T cycles

The ultrasonic pulse velocity (UPV) methodology serves as a quality control method for products intended to be composed of similar concrete, as it readily identifies both inadequate compaction and variations in the water/cement ratio [47]. Figure 15 illustrates the UPV measurements prior to and after to every 33 and 100 freeze-thaw cycles. As the number of freeze-thaw cycles increased, a decrease in the UPV values of all series was detected. Following 100 cycles, the UPV values for the G100, G92B8, G84B16, G76B24, G68B32, and G60B40

combinations were recorded as 1881, 1697, 1620, 1555, 1125, and 808 m/s, respectively. The UPV of the G100 mixture diminished by 11.7%. The UPV of the G92B8 combination containing 8% BP diminished by 15.7%. The UPV of the G84B16 combination containing 16% BP diminished by 18.22%. The reduction in the UPV of the 24% BP mixture was 17.7%. The reductions in the 32% and 40% BP mortars were 39.4% and 54.86%, respectively.

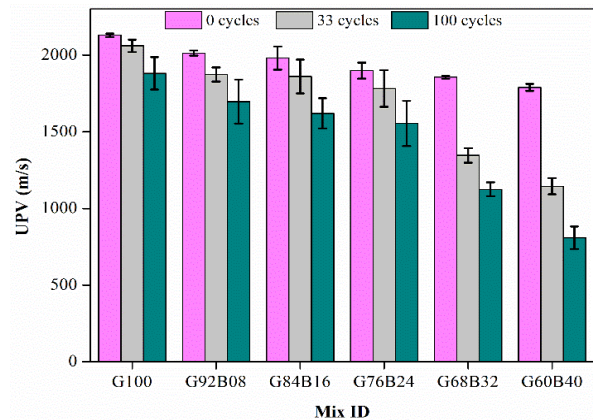


Figure 15. Average UPV before and after F-T cycles

Figure 16 shows compressive strength prior to and following 100 freeze-thaw cycles, along with the percentage changes in the mixtures. Following 100 freeze-thaw cycles, strength decreases of 9.89%, 28.66%, 27.88%, 37.5%, 49.81% and 61.61% were recorded in samples G100, G92B8, G84B16, G76B24, G68B32, and G60B40, respectively. The freeze-thaw impact resulted in a substantial 61.61% reduction in strength when the BP ratio reached 40%. After 100 freeze-thaw cycles, the significant decrease in strength was observed as the BP ratio (40%) increased, consistent with the highest decrease in UPV values (54.56%).

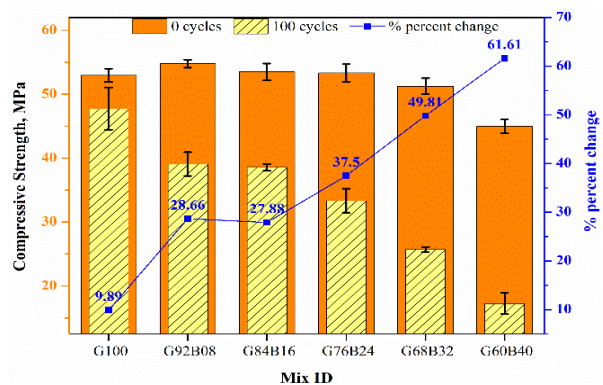


Figure 16. Change of compressive strength after F-T cycles

A correlation is evident among Figure 14, Figure 15 and Figure 16, illustrating the relationship between mass loss, UPV, and the drop in compressive strength following multiple freeze-thaw cycles. Figure 14 shows that only a small amount of material was lost. This small drop in weight showed that all AAMs had good structural stability after F-T cycles. However, the increase in mass loss with increasing BP replacement rate indicates that the matrix has poor long-term durability at high BP rates. Figure 15 illustrates UPV results indicating progressive declines following 33 and 100 F-T cycles, in alignment with the mass loss trend. UPV readings exhibited substantial reductions when BP content escalated.

The reduction in wave velocity signifies the formation of microcracks and interior structural degradation following F-T exposure. Figure 16 illustrates that the AAMs with 24%, 32%, and 40% BP underwent considerable strength degradation following 100 cycles. The control mix, G100, exhibited a strength reduction of 9.89%, but the 40% BP substitution levels resulted in more significant mechanical degradation. The reduction in compressive strength is closely associated with the UPV behaviour, hence validating the reliability of UPV as a non-destructive testing method.

3.5. Microstructural analyses

Microphotographs obtained from FIB-SEM analyses of G100 and G60B40 AAMs after 100 F-T cycles are shown in Figures 17a-17b. As seen in Figure 17a, the FIB-SEM image of the G100 sample reveals a compact structure consistent with the compressive strength, porosity, and water absorption values. As seen in Figure 17a, the FIB-SEM image of the G100 sample reveals a compact structure consistent with its compressive strength, porosity, and water absorption values. Figure 17b presents a microphotograph of the G60B40 sample, revealing microcracks with dimensions of 2.028 μm , 3.455 μm , 9.931 μm , and 5.841 μm . This image, as seen in the compressive strength, porosity, water absorption, and sorptivity results of G60B40, reveals a weaker microstructure than G100. Three distinct particle types were identified within the matrices of both samples:

entirely unreacted particles, particles that exhibited partial reaction, and interlocking particles that fully converted into geopolymer gel [48].

EDS analyses of G100 and G60B40 AAMs performed after 100 F-T exposure are given in Figures 17c-17d. The dominant elements detected in G100 are O (41.5%), Si (13.9%), Ca (13.5%), and Al (4.5%). The dominant elements in G60B40 mortar are O (46.3%), Si (14.1%), Ca (14%), and Al (4.7%). Ca, Si, and Al were predominantly detected in the matrix, supporting the formation of the C-A-S-H gel. The presence of GBFS, a high-calcium precursor material, in both EDS pictures accounts for the elevated Ca levels in the structure. This signifies that a gel structure rich in Ca, characteristic of alkali-activity, predominates the matrix, with the ensuing strengths contingent upon this gel structure. Prior research on basalt stone cutting waste demonstrates the emergence of both C-(N)-ASH gel (i.e., Ca-modified N-A-S-H gel) and C-A-S-H gel in these samples, attributable to the dissolution of calcium and its involvement in gel formation [49].

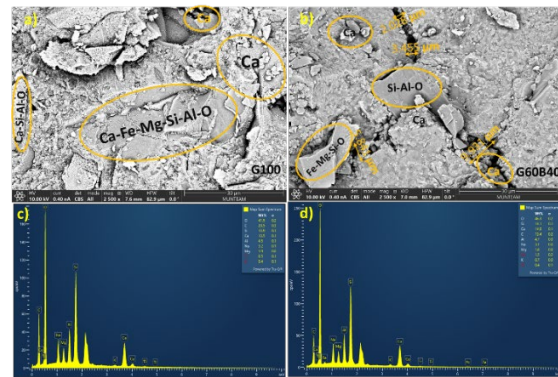


Figure 17. FIB-SEM/EDS images of a)-c) G100 and b)-d) G60B40 samples after F-T cycles

4. Conclusion

This study focused on the evaluation of the workability, mechanical, physical microstructure, and durability properties of alkali-activated mortars (AAM) containing basalt powder (BP) and granulated blast furnace slag (GBFS). Prismatic samples measuring 40x40x160 mm were produced for the experimental study. In these samples, BP was incorporated into the GBFS substitution at 8%, 16%, 24%, 32%, and 40%. The results are presented below.

- Increasing the BP content in the mixtures resulted in a decrease in fluidity.
- Adding up to 24% BP to a W/B ratio of 0.20 met the EFNARC criteria.
- Based on the 28-day compressive strength, the highest compressive strength was measured at 54.77 MPa in the G92B8 sample, while the lowest compressive strength was measured at 44.98 MPa in the G60B40 sample.
- Increasing the basalt powder content in the mixture increased both porosity and water absorption.
- A significant change in the average weight of the samples was recorded after 100 freeze-thaw cycles.
- However, after 100 freeze-thaw cycles, the greatest strength loss occurred in the G60B40 sample, at 61.61%, while the least loss was measured in the G100 sample, at 9.89%.
- Increasing the BP ratio in the mixture caused a decrease in the UPV values of the samples.
- The addition of BP negatively affected the microstructure of the matrix and reduced the resistance of the samples against F-T cycles.

As a result, this study recommends that BP should not be used more than 16% by weight in GBFS-based AAM

Article Information Form

Authors Contributions

Concept/Design, Data Analysis, Writing, Comprehensive Evaluation of Material, Literature Review: M.Ş.Y.; Data Collect, Experimental Works: S.C.

The Declaration of Conflict of Interest/ Common Interest

No conflict of interest or common interest has been declared by the authors.

Artificial Intelligence Statement

No artificial intelligence tools were used while writing this article.

Copyright Statement

Authors own the copyright of work published in the journal and work is published under the CC BY-NC 4.0 license.

References

- [1] Z. Q. Tang, H. Sui, F. B. de Souza, K. Sagoe-Crentsil, and W. Duan, "Silane-modified graphene oxide in geopolymer: Reaction kinetics, microstructure, and mechanical performance," *Cem. Concr. Compos*, vol. 139, p. 104997, May 2023. doi: 10.1016/j.cemconcomp.2023.104997. [Online]. <https://doi.org/10.1016/j.cemconcomp.2023.104997>
- [2] R. P. Singh, K. R. Vanapalli, K. Jadda, and B. Mohanty, "Durability assessment of fly ash, GGBS, and silica fume based geopolymer concrete with recycled aggregates against acid and sulfate attack," *J. Build. Eng*, vol. 82, p. 108354, Apr 2024. doi: 10.1016/j.job.2023.108354. [Online]. <https://doi.org/10.1016/j.job.2023.108354>
- [3] A. Singh, S. S. Bhadauria, A. A. Thakare, A. Kumar, M. Mudgal, and S. Chaudhary, "Durability assessment of mechanochemically activated geopolymer concrete with a low molarity alkali solution," *Case Stud. Constr. Mater*, vol. 20, p. e02715, July 2024. doi: 10.1016/j.cscm.2023.e02715. [Online]. <https://doi.org/10.1016/j.cscm.2023.e02715>
- [4] T. Cakmak, I. Ustabas, Z. Kurt, and E. Yilmaz, "Geopolymer mortars having glassy materials considering mechanical and microstructural features," *J. Build. Eng*, vol. 91, p. 109738, July 2024. doi: 10.1016/j.job.2024.109738. [Online]. <https://doi.org/10.1016/j.job.2024.109738>
- [5] J. P. Gill, V. S. Rathanasalam, P. Jangra, T. M. Pham, and D. K. Ashish, "Mechanical and microstructural properties of fly ash-based engineered geopolymer mortar

- incorporating waste marble powder," *Energy Ecol. Environ.*, vol. 9, no. 2, pp. 159–174, Apr 2024. doi: 10.1007/s40974-023-00296-3. [Online]. <http://dx.doi.org/10.1007/s40974-023-00296-3>
- [6] O. Y. Bayraktar, U. Yakupoglu, and A. Benli, "Slag/diatomite-based alkali-activated lightweight composites containing waste andesite sand: Mechanical, insulating, microstructural and durability properties," *Arch. Civ. Mech. Eng.*, vol. 23, no. 4, p. 248, Nov 2023. doi: 10.1007/s43452-023-00774-9. [Online]. <https://doi.org/10.1007/s43452-023-00774-9>
- [7] M. S. Nawab, T. Ali, M. Z. Qureshi, and O. Zaid, "A study on improving the performance of cement-based mortar with silica fume, metakaolin, and coconut fibers," *Case Stud. Constr. Mater.*, vol. 19, p. e02480, Dec 2023. doi: 10.1016/j.cscm.2023.e02480. [Online]. <https://doi.org/10.1016/j.cscm.2023.e02480>
- [8] Ü. Yurt and F. Bekar, "Comparative study of hazelnut-shell biomass ash and metakaolin to improve the performance of alkali-activated concrete: A sustainable greener alternative," *Constr. Build. Mater.*, vol. 320, p. 126230, Feb 2022. doi: 10.1016/j.conbuildmat.2021.126230. [Online]. <https://doi.org/10.1016/j.conbuildmat.2021.126230>
- [9] N. Gülmez, "Performance of marble powder on cementitious composites including waste steel chips as an additive," *Constr. Build. Mater.*, vol. 312, p. 125369, Dec 2021. doi: 10.1016/j.conbuildmat.2021.125369. [Online]. <https://doi.org/10.1016/j.conbuildmat.2021.125369>
- [10] A. Yılmaz, F. N. Degirmenci, and Y. Aygörmez, "Effect of initial curing conditions on the durability performance of low-calcium fly ash-based geopolymer mortars," *Bol. Soc. Esp. Ceram. Vidrio*, vol. 63, no. 4, pp. 238–254, July 2024. doi: 10.1016/j.bsecv.2023.10.006. [Online]. <https://doi.org/10.1016/j.bsecv.2023.10.006>
- [11] J. Davidovits, "Geopolymers," *J. Therm. Anal. Calorim.*, vol. 37, no. 8, pp. 1633–1656, Aug 1991. doi: 10.1007/bf01912193. [Online]. <https://doi.org/10.1007/bf01912193>
- [12] Ü. Yurt and M. Emiroğlu, "Zeolit İkameli Geopolimer Betonlarda Kür Şartlarının Etkileri," *Acad. Platform J. Eng. Sci.*, vol. 8, no. 2, pp. 396–402, May 2020. doi: 10.21541/apjes.688186. [Online]. <https://doi.org/10.21541/apjes.688186>
- [13] F. Arslan, A. Benli, and M. Karataş, "Effect of high temperature on the performance of self-compacting mortars produced with calcined kaolin and metakaolin," *Constr. Build. Mater.*, vol. 256, p. 119497, Sept 2020. doi: 10.1016/j.conbuildmat.2020.119497. [Online]. <https://doi.org/10.1016/j.conbuildmat.2020.119497>
- [14] M. Şahin Yön, "Mechanical, durability and microstructure properties of eco-friendly self-compacting mortars with addition of volcanic scoria, silica fume and boron waste as cement replacement," *Constr. Build. Mater.*, vol. 462, p. 139894, Feb 2025. doi: 10.1016/j.conbuildmat.2025.139894. [Online]. <https://doi.org/10.1016/j.conbuildmat.2025.139894>
- [15] M. Şahin Yön and M. Karataş, "Resistance to magnesium sulphate attack of binary and ternary cementless self-compacting alkali-activated mortar," *J. Build. Eng.*, vol. 95, p. 109988, Oct 2024. doi: 10.1016/j.job.2024.109988. [Online]. <https://doi.org/10.1016/j.job.2024.109988>

- [16] C. Lu, Z. Zhang, C. Shi, N. Li, D. Jiao, and Q. Yuan, "Rheology of alkali-activated materials: A review," *Cem. Concr. Compos*, vol. 121, p. 104061, Aug 2021. doi: 10.1016/j.cemconcomp.2021.104061. [Online]. <https://doi.org/10.1016/j.cemconcomp.2021.104061>
- [17] D. M. Roy, W. Jiang, and M. R. Silsbee, "Chloride diffusion in ordinary, blended, and alkali-activated cement pastes and its relation to other properties," *Cem. Concr. Res.*, vol. 30, no. 12, pp. 1879-1884, Dec 2000. doi: 10.1016/S0008-8846(00)00406-3. [Online]. [https://doi.org/10.1016/S0008-8846\(00\)00406-3](https://doi.org/10.1016/S0008-8846(00)00406-3)
- [18] J. L. Provis, P. Duxson, J. S. J. van Deventer, and G. C. Lukey, "The role of mathematical modelling and gel chemistry in advancing geopolymer technology," *Chem. Eng. Res. Des.* vol. 83, no. 7A, pp. 853-860, July 2005. doi: 10.1205/cherd.04329. [Online]. <https://doi.org/10.1205/cherd.04329>
- [19] M. Wankhede and R. Ralegaonkar, "Development of one-part alkali-activated mortar using foundry waste sand," *Adv. Civ. Eng.*, vol. 2025, no. 1, p. 9045753, Jan 2025. doi: 10.1155/adce/9045753. [Online]. <https://doi.org/10.1155/adce/9045753>
- [20] A. Mobili, E. Blasi, Q. Maqbool, and F. Tittarelli, "Copper mine tailings and metakaolin as precursors for sustainable alkali-activated mortars," *J. Build. Eng.*, vol. 103, p. 112134, Jan 2025. doi: 10.1016/j.jobe.2025.112134. [Online]. <https://doi.org/10.1016/j.jobe.2025.112134>
- [21] Z. Ma, Y. Wu, K. Fang, Y. Zhang, and C. Wang, "Developing fully recycled alkali-activated mortar made with waste concrete fines as a substitute for both binder and sand: multi-properties evaluation," *Constr. Build. Mater.*, vol. 477, p. 141323, May 2025. doi: 10.1016/j.conbuildmat.2025.141323. [Online]. <https://doi.org/10.1016/j.conbuildmat.2025.141323>
- [22] Y. Guo, X. Xu, and W. Guo, "Effect of alkaline activator on SIOT-GGBS-MK based alkali-activated mortar," *Constr. Build. Mater.*, vol. 467, p. 140322, Mar 2025. doi: 10.1016/j.conbuildmat.2025.140322. [Online]. <https://doi.org/10.1016/j.conbuildmat.2025.140322>
- [23] Ü. Yurt and H. Bayraktar, "Towards innovative and sustainable building materials: Effect of alkali activator concentration on the performance of waste brick powder-based geopolymer composites," *Environ. Res.*, vol. 283, p. 122109, Apr 2025. doi: 10.1016/j.envres.2025.122109. [Online]. <https://doi.org/10.1016/j.envres.2025.122109>
- [24] Ü. Yurt, "High performance cementless composites from alkali activated GGBFS," *Constr. Build. Mater.*, vol. 264, p. 120222, Dec 2020. doi: 10.1016/j.conbuildmat.2020.120222. [Online]. <https://doi.org/10.1016/j.conbuildmat.2020.120222>
- [25] D. Mrozek, M. Mrozek, and R. Krzywoń, "Mechanical properties of geopolymers synthesized using basalt powder as a partial substitute for metakaolin," *Sci. Rep.*, vol. 15, no. 1, p. 13156, Jan 2025. doi: 10.1038/s41598-025-96447-z. [Online]. <https://doi.org/10.1038/s41598-025-96447-z>
- [26] A. M. Rashad, M. H. El-Nashar, and F. A. Z. Refaie, "From Egyptian stone to sustainable binder: The impact of basalt powder on metakaolin geopolymer cement," *Edelweiss Appl. Sci. Technol.*, vol. 9, no. 9, pp. 1268-1287, 2025. doi: 10.55214/2576-8484.v9i9.10127. [Online]. <https://learning-gate.com/index.php/2576-8484/article/view/10127/3288>

- [27] M. Łach, B. Kozub, S. Bednarz, A. Bąk, M. Melnychuk, and A. Masłoń, "The influence of the addition of basalt powder on the properties of foamed geopolymers," *Materials*, vol. 17, no. 10, p. 2336, May 2024. doi: 10.3390/ma17102336. [Online]. <https://doi.org/10.3390/ma17102336>
- [28] Ü. Yurt, S. Çelikten, and İ. İ. Atabey, "Post-fire residual mechanical and microstructural properties of waste basalt and glass powder-based geopolymer mortars," *J. Build. Eng.*, vol. 94, p. 109941, Oct 2024. Doi: 10.1016/j.jobe.2024.109941. [Online]. <https://doi.org/10.1016/j.jobe.2024.109941>
- [29] M. Şahin Yön and M. Karataş, "Evaluation of the mechanical properties and durability of self-compacting alkali-activated mortar made from boron waste and granulated blast furnace slag," *J. Build. Eng.*, vol. 61, p. 105263, Dec 2022. doi: 10.1016/j.jobe.2022.105263. [Online]. <https://doi.org/10.1016/j.jobe.2022.105263>
- [30] D. Hardjito, S. E. Wallah, D. M. J. Sumajouw, and B. V. Rangan, "On the development of fly ash-based geopolymer concrete," *ACI Mater. J.*, vol. 101, no. 6, pp. 467-472, Nov 2004. doi: Not available [Online]. https://www.researchgate.net/profile/Djwan-ntoro-Hardjito/publication/303836414_ACI_Materials/links/5c7c43bd92851c6950520ea1/ACI-Materials.pdf
- [31] J. Temuujin, R. P. Williams, and A. V. Van Riessen, "Effect of mechanical activation of fly ash on the properties of geopolymer cured at ambient temperature," *J. Mater. Process. Technol.*, vol. 209, no. 12-13, pp. 5276-5280, July 2009. doi: 10.1016/j.jmatprotec.2009.03.016. [Online]. <https://doi.org/10.1016/j.jmatprotec.2009.03.016>
- [32] *The European guidelines for self-compacting concrete: Specification, production and use*, EFNARC, U.K., May 2002.
- [33] *Standard Test Method for Flexural Strength of Hydraulic-Cement Mortars*, ASTM C348, ASTM Int., West Conshohocken, PA, USA, 2002.
- [34] *Standard Test Method for Compressive Strength of Hydraulic-Cement Mortars (Using Portions of Prisms Broken in Flexure)*, ASTM C349, ASTM Int., West Conshohocken, PA, USA, 2002.
- [35] *Standard Test Method for Measurement of Rate of Absorption of Water by Hydraulic-Cement Concretes*, ASTM C1585-04, ASTM Int., West Conshohocken, PA, USA, 2007.
- [36] *Standard Test Method for Resistance of Concrete to Rapid Freezing and Thawing*, ASTM C666/C666M, ASTM Int., West Conshohocken, PA, USA, 2003.
- [37] A. M. Rashad, R. A. E. Mohamed, S. R. Zeedan, and A. A. El-Gamal, "Basalt powder as a promising candidate material for improving the properties of fly ash geopolymer cement," *Constr. Build. Mater.*, vol. 435, 136805, July 2024. doi: 10.1016/j.conbuildmat.2024.136805. [Online]. <https://doi.org/10.1016/j.conbuildmat.2024.136805>
- [38] B. Ngayakamo and S. Christiansen, "Eco-friendly metakaolin-basalt geopolymer blocks: A sustainable building material alternative," *Next Sustain*, vol. 6, p. 100188, Jan 2025. doi: 10.1016/j.nxsust.2025.100188. [Online]. <https://doi.org/10.1016/j.nxsust.2025.100188>
- [39] S. Çelikten and M. B. Çavuşoğlu, "Mechanical and microstructural properties of fiber-reinforced basalt rock cutting waste-based geopolymer composites exposed to high temperatures,"

- Environ. Sci. Pollut. Res.*, vol. 32, no. 7, pp. 3629–3648, Feb 2025. doi: 10.1007/s11356-025-35916-4. [Online]. <https://doi.org/10.1007/s11356-025-35916-4>
- [40] F. Servadei, N. Cotineau, V. Medri, A. N. Murri, E. Papa, G. Valdrè, and E. Landi, "Co-valorisation of construction and demolition waste and basalt powder as raw materials in geopolymers," *Constr. Build. Mater.*, vol. 492, p. 143009, Sep 2025. doi: 10.1016/j.conbuildmat.2025.143009. [Online]. <https://doi.org/10.1016/j.conbuildmat.2025.143009>
- [41] P. Venyite, E. C. Makone, R. C. Kaze, A. Nana, J. G. D. Nemaleu, E., Kamseu, U. C. Melo, and C. Leonelli, "Effect of combined metakaolin and basalt powder additions to laterite-based geopolymers activated by rice husk ash (RHA)/NaOH solution," *Silicon*, vol. 14, no. 4, pp. 1643-1662, Mar 2022. doi: 10.1007/s12633-021-00950-7. [Online]. <https://doi.org/10.1007/s12633-021-00950-7>
- [42] C. Hall, "Water sorptivity of mortars and concretes: A review," *Mag. Concr. Res.*, vol. 41, no. 147, pp. 51-61, June 1989. doi: 10.1680/mac.1989.41.147.51. [Online]. <https://doi.org/10.1680/mac.1989.41.147.51>
- [43] U. K. Sevim, M. Ozturk, S. Onturk, and M. B. Bankir, "Utilization of boron waste borogypsum in mortar," *J. Build. Eng.*, vol. 22, pp. 496-503, Mar 2019. doi: 10.1016/j.job.2019.01.015. [Online]. <https://doi.org/10.1016/j.job.2019.01.015>
- [44] H. Alanazi, M. Yang, D. Zhang, and Z. Gao, "Early strength and durability of metakaolin-based geopolymer concrete," *Mag. Concr. Res.*, vol. 69, no. 1, pp. 46-54, Jan 2017. doi: 10.1680/jmacr.16.00118. [Online]. <https://doi.org/10.1680/jmacr.16.00118>
- [45] T. A. Aiken, J. Kwasny, W. Sha, and K. T. Tong, "Mechanical and durability properties of alkali-activated fly ash concrete with increasing slag content," *Constr. Build. Mater.*, vol. 301, p. 124330, Oct. 2021. doi: 10.1016/j.conbuildmat.2021.124330. [Online]. <https://doi.org/10.1016/j.conbuildmat.2021.124330>
- [46] M. Şahin Yön, B. Yön, M. Karataş, and A. Benli, "Sustainable use of boron waste and volcanic scoria in slag-based self-compacting alkali-activated mortars: Fresh, mechanical and durability properties," *Sustain. Chem. Pharm.*, vol. 41, p. 101550, Oct 2024. doi: 10.1016/j.scp.2024.101664. [Online]. <https://doi.org/10.1016/j.scp.2024.101664>
- [47] R. Demirboğa, I. Türkmen, and M. B. Karakoç, "Relationship between ultrasonic velocity and compressive strength for high-volume mineral-admixtured concrete," *Cem. Concr. Res.*, vol. 34, no. 12, pp. 2329–2336, Dec 2004. doi: 10.1016/j.cemconres.2004.04.017. [Online]. <https://doi.org/10.1016/j.cemconres.2004.04.017>
- [48] G. F. Huseien, A. R. M. Sam, K. W. Shah, and J. Mirza, "Effects of ceramic tile powder waste on properties of self-compacted alkali-activated concrete," *Constr. Build. Mater.*, vol. 236, p. 117574, Feb 2020. doi: 10.1016/j.conbuildmat.2019.117574. [Online]. <https://doi.org/10.1016/j.conbuildmat.2019.117574>
- [49] B. Işıkdag and S. Çelikten, "The effect of basalt stone cutting waste on the high-temperature performance of fly ash-based geopolymers," *J. Build. Eng.*, vol. 113, p. 114040, Jan 2025. doi: 10.1016/j.job.2025.114040. [Online]. <https://doi.org/10.1016/j.job.2025.114040>